Low Temperature Physics/Fizika Nizkikh Temperatur, 2019, v. 45, No. 7, pp. 807–815

Bi_2Ne: Weakly bound cluster of diatomic bismuth with neon

A. Endo[1], M. Hatanaka[2,3], N. Ueno[1], Y. Morisawa[1], and T. Wakabayashi[1]

[1]*Department of Chemistry, School of Science and Engineering, Kindai University, Higashi-Osaka 577-8502, Japan*

[2]*Institute for Research Initiatives, Graduate School of Science and Technology, and Data Science Center, Nara Institute of Science and Technology (NAIST), Ikoma 630-0192, Japan*

[3]*PRESTO, Japan Science and Technology Agency (JST), Kawaguchi 332-0012, Japan*

E-mail: wakaba@chem.kindai.ac.jp

Received January 6, 2019, published online May 28, 2019

The *A*–*X* transition of diatomic bismuth, Bi_2, was revisited by laser induced fluorescence in solid Ne at 3 K. Molecular constants, i.e., vibrational frequencies of 137 cm^{-1} and 174 cm^{-1}, were reproduced for the upper and lower electronic states as reported by Bondybey *et al*. [*Chem. Phys. Lett.* **76**, 30 (1980)]. Two-dimensional mapping of emission spectra confirmed satellite bands in higher and lower excitation/emission energies for each of the major bands in the vibrational progression of v'–v'' (v' = 0–5, v'' = 5–12). Based on the molecular orbital calculations, presence of clusters, Bi_2Ne_n (n = 1–6), is proposed for possible carriers of the observed satellites. For the relatively large matrix shift of ~ 67 cm^{-1} in solid Ne for the term energy of the *A* state, the diatomic bismuth is supposed to exist as a linearly coordinated cluster of Bi_2Ne in the matrix.

Keywords: bound cluster, fluorescence, diatomic bismuth.

1. Introduction

The *A*–*X* system of diatomic bismuth, Bi_2, is one of the most explored transition systems among those in the homonuclear diatomic molecules [1–6]. For its heavy constituent atoms, i.e., a single isotope of ^{209}Bi in the $^4S_{3/2}$ ground state stemming from the $(6s)^2(6p)^3$ configuration having a nuclear spin of I = 9/2, Bi_2 is thought as the most complex dimer in the periodic table. Due to strong spin-orbit coupling, several electronic states originating from the mixture of spin-singlet and -triplet states are known to exist above the ground state up to 36500 cm^{-1} [1,2]. The *A*–*X* transition having the 0–0 band at 17719 cm^{-1} in the gas phase has been extensively studied as the lowest-energy fully allowed transition from the ground state, *X* [1–6]. With relatively low harmonic frequencies, ω'_e = 132 cm^{-1} in the upper electronic state, *A*, and ω''_e = 173 cm^{-1} in the lower electronic state, *X*, the optical emission spectra exhibit extensive vibrational progression accompanied by numerous lines due to rotational structures [4–6]. A number of robivronic emission lines of gaseous Bi_2 spans whole visible ranges depending on the excitation wavelength at high temperature conditions above 800 °C, which is necessary for producing sufficient vapor pressure for the diatomic bismuth.

Matrix-isolated Bi_2 has also been a spectroscopic target in addition to gaseous one [7–14]. As a result of the frozen rotational degrees of freedom in such a condensed phase of solid Ne, Ar, Kr, Xe, or N_2, spectra are observed with a simple vibrational progression of Bi_2, though spectral lines are shifted and broadened compared to those in the gas phase. When the molecular structure, i.e., the internuclear distance for a diatomic molecule, is modified in the condensed matrix so as to minimize the energy in its ground state through the interaction with the inert but contact matrix atoms or molecules, transition energy in the matrix is typically blue-shifted compared to that in the gas phase. Concerning the *A*–*X* transition of Bi_2, its 0–0 band was located at 17786 cm^{-1} in solid Ne as blue-shifted by ~ 67 cm^{-1} [9]. Using solid Ar matrices, controversial assignments had been made for the *A*–*X* transition as well as for the other electronic transitions of Bi_2 [10]. One thing that had led to such a controversy was the lack of direct observation of the 0–0 band in the *A*–*X* transition in those matrices. It was also noted that a relatively large Franck–Condon shift for the *A*–*X* system of Bi_2, showing the maximum fluorescence intensity at the 0–8 band, prevented the observation of the 0–0 band in noticeable intensity. The agreement with the gas-phase data had not been reached indeed, until the series of Raman spectroscopic studies could identify the

vibrational frequency of ~173 cm^{-1} in the matrix [9,11–14]. Molecular constants for low-lying electronic states of Bi_2 are summarized in the literature [1].

Recently, near infrared emission spectra for the neutral triatomic bismuth, Bi_3, were newly detected in solid Ne [15] and successfully identified to locate four low-lying electronic excited states at 1870, 8470, 9625, and 11395 cm^{-1} above the ground state [16]. The lowest one is the split spin-orbit counterpart to the ground state, while the upper two levels are the spin-orbit components of another electronic state. These features coincide well with the photoelectron spectra (PES) of the trimer anion, Bi_3^-, in the gas phase [17]. The excited state at 9625 cm^{-1} in solid Ne is identical with the one observed in the resonant two-photon ionization (R2PI) spectra [18]. Theoretical considerations have been made for the relativistic effect in the spin-mixed states [19–22]. Recently, evolution of molecular structures of larger clusters, Bi_n ($n \geq 2$), has been studied theoretically [23–26] and experimentally [27,28]. A major advantage for the laser induced optical emission spectroscopy is its high sensitivity, accessible in combination with low-temperature condensed matrices containing relatively high-density target molecules. Matrix isolation spectroscopy is applicable also to the bismuth dimer, Bi_2, as well as the trimer, Bi_3 [15,16].

We revisited spectroscopy of the *A*–*X* transition in Bi_2 embedded in solid Ne matrices by laser induced fluorescence mapping to extend the observation of the series of vibronic transitions. Molecular constants including the term energy, T_e, as well as the transition energy for the 0–0 band, ν_{00}, and vibrational harmonic frequencies, ω'_e in the upper *A* state and ω''_e in the lower *X* state, are compared with those reported in solid Ne [9] and in the gas phase [1,4]. Moreover, in the fluorescence-mapping pattern, we found a series of satellites associated with the *A*–*X* system of Bi_2 in solid Ne, where a luminescent spot for the vibronic transition is accompanied by a train of dim spots with an increment of ~50 cm^{-1} in the lower excitation/emission energies and increments of ~30 cm^{-1} and ~10 cm^{-1} in the higher excitation/emission energies. We will discuss about the systematic pattern observed in the photoluminescence (PL) excitation-emission mapping in the visible wavelength range for getting insight into dynamical aspects of the diatomic molecule of Bi_2 in terms of the weak interaction with surrounding neon atoms in the condensed phase.

2. Experiments

2.1. Matrix sample of Bi_2 in solid Ne

Matrix isolation technique was employed as described elsewhere [15,16,29,30]. Briefly, granular bismuth (Nilaco Bi 99.9999%) was placed inside a molybdenum-covered crucible and heated in vacuum to ~1000 K. Bismuth vapor molecules as well as atoms were emanated from the crucible, monitored by using quadrupole mass spectrometer with electron ionization (Extrel QMS MAX500), and deposited on the cold surface cooled at ~3 K (Sumitomo RDK-205D), together with excess neon gas to form a solid Ne matrix sample containing small amount of Bi, Bi_2, and Bi_3 [15,16,29]. The matrix sample was a few millimeters thick and colorless, containing the atomic and molecular bismuth typically to the extent up to an atomic ratio of 1:1000 for Bi:Ne.

2.2. Laser-induced fluorescence (LIF)

For the selective excitation of Bi_2, tunable pulsed dye laser was used for photoexcitation (Sirarh Cobra Stretch, ~1 mJ/pulse, pumped by second/third harmonics of Nd:YAG, Spectra Physics INDI 40 operated at 10 Hz). Since the linewidth of absorption as well as emission was relatively narrow, increments for the excitation were necessarily to set as narrow as possible. Excitation was made at every 0.1 nm increments within a range of 565.6–540.0 nm using pyrromethane 580 excited at 532 nm for the excitation of vibrational $v' = 0, 1, 2$ levels in the upper electronic state, namely *A*, and coumarin 153 excited at 355 nm for the excitation of $v' = 3, 4, 5$ levels in *A*. Dispersed fluorescence spectra for 0–v'' bands of $v'' = 4$–12 in the *A*–*X* transition were recorded in a spectral range of 580–700 nm with a resolution of 0.1 nm by using a spectrometer (Acton SP300i, 600 G/mm blazed at 1000 nm) equipped with a CCD-array detector (PI SPEC-10). To reduce stray light, a long-pass color glass filter (Schott OG590) was placed before the entrance slit of the spectrometer. Close to the origin band, ν_{00}, of the *A*–*X* transition of Bi_2 at the excitation of 17786 cm^{-1} (562.1 nm) in solid Ne, part of the emission features below the cut-off wavelength, i.e., 590 nm, were artificially diminished in their intensities.

The observed series of emission spectra was reconstructed as a two-dimensional fluorescence excitation mapping using a graph-drawing software, Igor ver. 6.3. The 2D-fluorescence mapping enables the detection of faint signals by discriminating a dim spot from the flat surface of a monotonous color. With this representation, we successfully identified satellite bands associated with each vibronic band in the *A*–*X* system of Bi_2.

3. Theory

3.1. The A–X system of Bi_2

The *A*–*X* system of Bi_2 is the lowest-energy fully allowed transition of the homonuclear diatomic molecule, $A^1 0_u^+ – X^1 0_g^+$ in the $D_{\infty h}$ point group symmetry. Due to strong spin-orbit coupling, triplet states, even quintet states as well, can be mixed in both the excited and the ground states [1,19–22]. Some low-lying excited states below the *A* state at T_e = 17739 cm^{-1} have been reported by emission and absorption [1].

Figure 1 illustrates the potential curves for the upper electronic state, *A*, and the lower electronic state, *X*. Vibrational levels are indicated by horizontal lines on the poten-

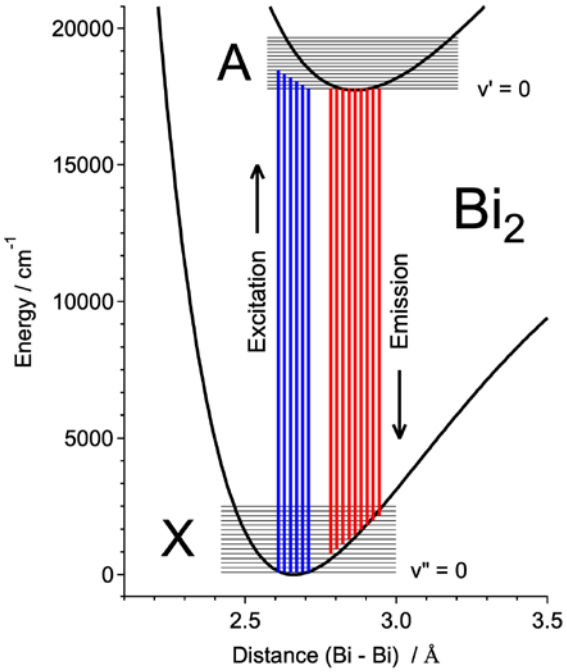

Fig. 1. Vibronic energy levels for the *A*–*X* system of Bi_2.

tial curve of each electronic state. The harmonic frequency in the gas phase is ω_e'' = 173.01 cm^{-1} for the ground state, *X*, while ω_e' = 132.66 cm^{-1} for the excited state, *A* [1]. For the low-frequency vibration of the Bi–Bi bond due to heavy constituent atoms, vibrational levels are well described by harmonic patterns to the higher vibrational quantum number of $v > 10$. Nevertheless, correction is needed for anharmonicity, as represented by the following formula in the unit of cm^{-1} [31];

$$E(A) = T_e + \omega_e'\left(v' + \frac{1}{2}\right) - \omega_e x_e'\left(v' + \frac{1}{2}\right)^2,$$

and

$$E(X) = \omega_e''\left(v'' + \frac{1}{2}\right) - \omega_e x_e''\left(v'' + \frac{1}{2}\right)^2.$$

The excitation performed in the present work is indicated by six vertical lines in blue in Fig. 1 from $v'' = 0$ in *X* to $v' = 0$–5 in *A*, while the observed emission bands are indicated by nine vertical lines in red for 0– v'' of $v' = 4$–12 with a progression in the lower state, *X*. For the latter transitions where the upper vibrational level is fixed, $v' = 0$, transition energy, ΔE, is represented as follows;

$$\Delta E = E(A) - E(X) = \nu_{00} - \omega_e'' v'' + \omega_e x_e''\left(v'' + \frac{1}{2}\right)^2,$$

where

$$\nu_{00} = T_e + \frac{1}{2}\left(\omega_e' - \omega_e''\right) - \frac{1}{4}\omega_e x_e'.$$

Experimental data of dispersed fluorescence spectra were fitted by using these equations to deduce molecular constants, ω_e'' and $\omega_e x_e''$ in the lower *X* state. Fluorescence excitation spectra were analyzed for the molecular constants in the upper *A* state, namely vibrational constants, ω_e' and $\omega_e x_e'$, and the electronic term energy, T_e.

3.2. Molecular orbital calculations

Molecular orbital calculations were performed for the weak interaction of Bi_2 and Ne by using a pseud core potential (ECP), i.e., B3LYP/GENECP, ECP78MDF for Bi and 6-31++G* for Ne [32]. In order to elucidate the landscape of the potential surface of a Ne atom around a diatomic Bi_2, calculated energies are plotted in a 2D-map along the coordinates in a cross section of the cylindrical coordinates.

4. Results

4.1. The A–X transition in Bi_2

Figure 2 shows a series of dispersed emission spectra of 0–v'' bands (v'' = 4–12) in the *A*–*X* transition of Bi_2 in solid Ne at 3 K. Conspicuous vibrational progression with an increment of ~170 cm^{-1} showing a substantial Franck–Condon shift promises the presence of the spectral carrier,

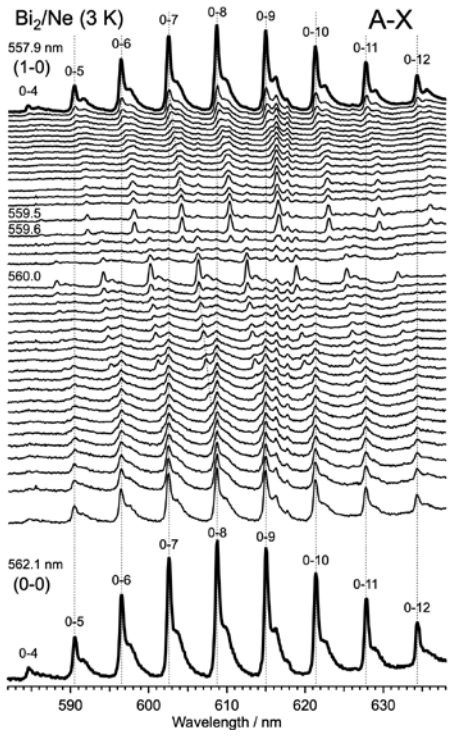

Fig. 2. Dispersed fluorescence spectra of the *A*–*X* system in Bi_2 in solid Ne at 3 K. Each spectrum corresponds to the laser excitation at a particular wavelength of every 0.1 nm in a range of 562.1–557.9 nm. Besides the strong fluorescence signals for the 0–0 and 1–0 excitation at 562.1 and 557.9 nm, respectively, weaker signals are noticeable in between these excitation wavelengths.

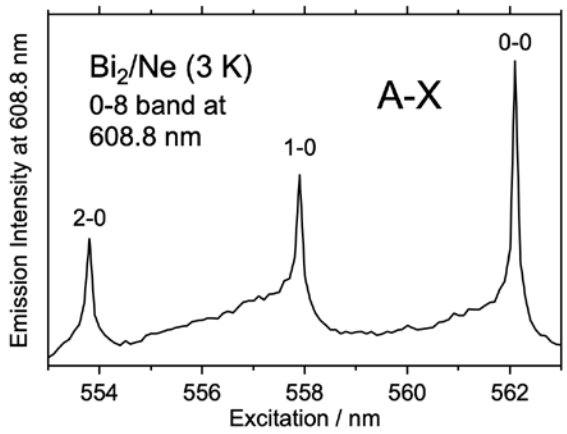

Fig. 3. Excitation spectrum of the *A*–*X* transition of Bi_2 in solid Ne at 3 K. The emission intensity at 608.8 nm for the 0–8 band is plotted as a function of the excitation wavelength.

Bi_2, in its ground state, *X* [1,9]. With the excitation at 562.1 nm, intensity of these bands was maximum (bottom trace), while the second maximum was at 557.9 nm (uppermost trace), where the spectral features were almost identical with those at 562.1 nm. They are attributable to the excitation of 0–0 and 1–0 transitions in the *A*–*X* system. The interval of ~134 cm^{-1} for the two excitation wavelengths coincides well with the vibrational frequency in the *A* state [1,9]. Similar spectral patterns appear repetitively at the excitation wavelength of 553.8 nm for the 2–0 transition.

Figure 3 shows the fluorescence excitation spectrum, obtained by plotting the emission intensity at the peak maximum of the 0–8 transition at 608.8 nm as a function of the excitation wavelength. The vibrational progression of ~134 cm^{-1} is noted for the vibrational frequency in the upper *A* state of Bi_2 [1,9]. Relative intensity is governed by the probability of internal conversion toward the vibrational $v' = 0$ level within the manifold of the *A* state. The strongest 0–0 band is reasonable because the monitoring band is the transition from the $v' = 0$ level in the upper state, which is the same vibrational level for the excitation. Molecular constants derived from transition energies for the *A*–*X* system of Bi_2 in solid Ne at 3 K are summarized in Table 1. Fitting was made by peaks in the excitation spectra, v'–0 ($v' = 0$–5), for the molecular constants in the excited state, *A*, and by peaks in the emission spectra, 0–v'' ($v'' = 5$–12), for the molecular constants in the ground state, *X*.

Table 1. Molecular constants in cm^{-1} for Bi_2 in solid Ne (this work)

State	T_e	ω_e	$\omega_e x_e$
A	17811 ± 1.4	137 ± 1.2	0.75 ± 1.0
X	0	174.2 ± 0.5	0.42 ± 0.03

4.2. Satellite bands

Traces depicted between the two spectra in Fig. 2 are those observed by the excitation at every 0.1 nm between the two wavelengths of 562.1 nm and 557.9 nm. From bottom, the main feature by the 0–0 excitation diminishes and the same feature emerges by the 1–0 excitation to the top. In addition, weaker features are appearing toward the excitation wavelength of 560.0 nm. These peaks show blue shifts upon increasing excitation energy from bottom, deviating into shorter wavelengths from the major peak upon the 0–0 excitation at 562.1 nm. Starting at the excitation of 559.6 nm, another weak feature is appearing as blue-shifting to merge into the major peak upon the 1–0 excitation at 557.9 nm. Each vibronic band of 0–v'' ($v'' = 5$–12) in emission is accompanied by similar features. All the minor peaks, noticeable as satellites, can be associated with particular vibronic bands in the *A*–*X* system of Bi_2. Considering the number of vibrational degrees of freedom, diatomic molecule having only one vibrational mode is insufficient to explain the observed additional spectral feature.

For the pattern of satellites in more detail, the series of emission spectra are plotted in a two-dimensional map in Fig. 4, for showing the emission intensity in colors as functions of excitation and emission energies in cm^{-1}. Red spots horizontally aligned at levels of the excitation energy of 17790 cm^{-1} and 17924 cm^{-1} correspond to the series of strong emission bands of 0–v'' upon the excitation of the 0–0 and 1–0 bands, respectively. The same 0–v'' emission upon the excitation of the 2–0 band is also discernible at 18057 cm^{-1}. Each of the major spots, i.e., the 0–v'' bands, is accompanied by a series of weak satellites to upper left and to lower right. Each series of satellites constitute a train of spots, i.e., several in the upper left and a few in the lower right.

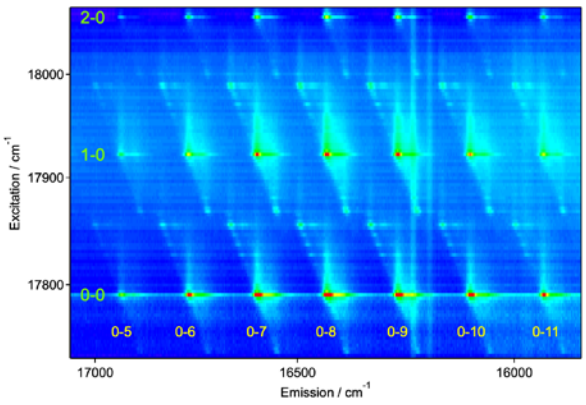

Fig. 4. (Color online) 2D-map of the emission intensity for the *A*–*X* transition of Bi_2 in solid Ne at 3 K. The interval of ~134 cm^{-1} for the excitation between 1–0 and 0–0 bands represents the vibrational frequency in the excited *A* state, while that of ~170 cm^{-1} for the emission between 0–7 and 0–8 bands the frequency in the ground *X* state. Each vibronic band is accompanied by a weaker series of satellite bands.

Appearing as a spot in the fluorescence mapping in Fig. 4, the satellite is ascribed as the signal of the species having one-to-one correspondence in the excitation and emission energies. Moreover, the number of satellites for each band is limited to five in the higher excitation/emission energies and only one in the lower excitation/emission energies. Furthermore, among the series of spots associated with a particular band of 0–v'', the major peak of the strongest intensity (red spot) is located in the middle of the line on which the satellites as well as the major peak are located. To understand these observations, discussions are necessary along the role of interaction between Bi_2 and Ne.

5. Discussion

5.1. Fluorescence excitation and emission

To see the satellite bands in more detail, Fig. 5 depicts a close-up view of a part of the 2D-map in Fig. 4. The weak satellites as well as the major peak, all associated with the 0–8 transition, are aligned along the dotted line in yellow in the left panel of Fig. 5. Besides the strong red spot, namely *b*, satellites are discernible as five spots, *c*–*g*, in higher energies both in excitation and emission and as one spot, *a*, in lower energies both in excitation and emission. Similar patterns are confirmed for the adjacent series of satellites and a major peak for the 0–7 and 0–9 transitions. The magnitude of inclination for the dotted line is close to unity, which means the energy shift in emission is almost the same as the energy shift in excitation.

The right panel in Fig. 5 plots the emission intensity along the dotted line in the left panel in Fig. 5. Commonly for three traces associated with the 0–7, 0–8, and 0–9 transitions, satellites, *a* and *c*–*g*, are peaking at lower and higher energies of the major peak, *b*. For solid lines, the signals are projected on the axis of excitation energy, where an offset is adopted to make the energy of the lowest-energy satellite, *a*, zero. The satellite, *a*, is lower in the excitation energy by 52 cm^{-1} than the major peak, *b*, while the other five, *c*–*g*, are higher by 28–68 cm^{-1} with a common increment of ~10 cm^{-1}. The projection to the axis of emission energy reproduces the same pattern but with slightly smaller increments as plotted by dotted lines in the right panel in Fig. 5. For higher vibrational quantum numbers, v'', separation in cm^{-1} between the satellite peaks diminishes, indicating slightly deviating vibrational constants for the carrier of satellites.

5.2. Weakly bound cluster of Bi_2–Ne

For the explanation of the satellites, vibrational transitions of Bi_2, including high-v' and high-v'' levels, were examined to create no series of transitions which reproduce a uniform increment of ~10 cm^{-1}. A series of hot-band excitations, namely transitions from the vibrational v'' level in the lower *X* state to the vibrational $v'' - 1$ level in the upper *A* state, might exhibit a difference of $\omega''_e - \omega'_e$ = 174–137 = = 37 cm^{-1}, but the observed increment was four times smaller for the resonance excitation. Even under considerations of anharmonicities in the upper and lower electronic states, the regular increment of ~10 cm^{-1} was not reproduced. The satellites are not explainable by the vibrational degree of freedom of Bi_2 alone.

The observations to be explained are the followings: (1) Increasing (decreasing) excitation energy is coupled by increasing (decreasing) emission energy. This trend simply indicates the energy shift of the upper and lower electronic potentials. Also, it is noted here that the lowest-energy satellite, *a*, at 17738 cm^{-1} is closely locating to the position of the gas-phase transition energy for the 0–0 band at

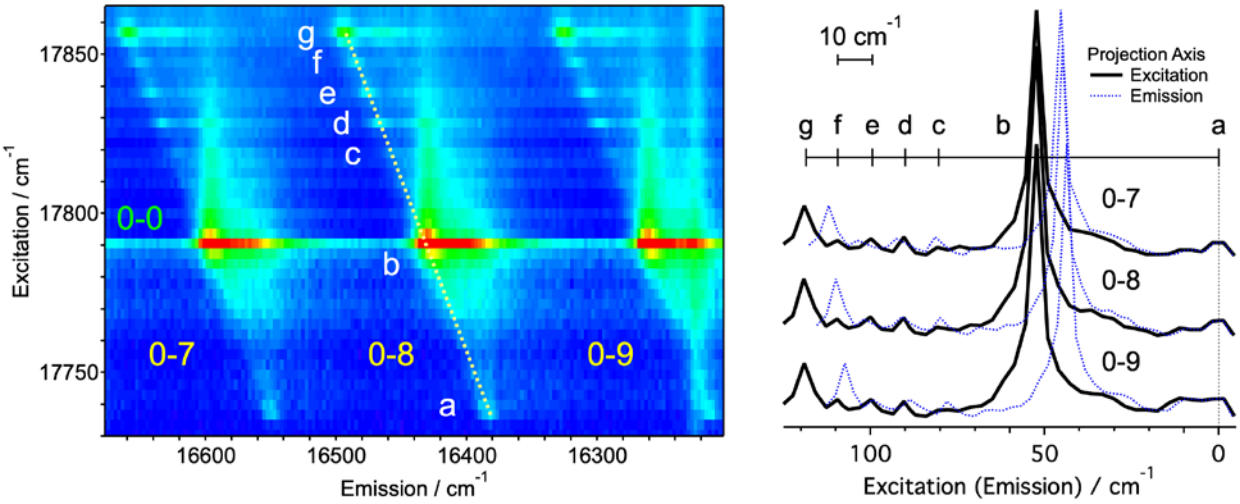

Fig. 5. (Color online) Close-up view of the 2D-map of the *A*–*X* transition of Bi_2 in solid Ne at 3 K (left panel), showing a group of satellite bands in the higher, *c*–*g*, and lower, *a*, frequencies of the main band, *b*. Projection of the emission intensity along the dotted line in the 2D-map (right panel), depicting the satellites, *a* and *c*–*g*, separated from the main band, *b*, by a multiple of an increment of ~10 cm^{-1}.

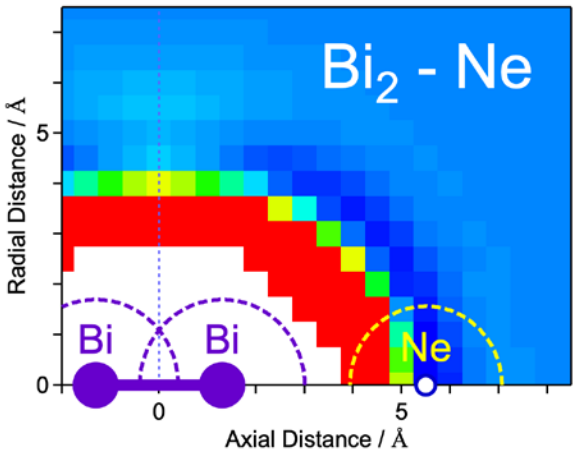

Fig. 6. (Color online) Potential surface of Bi_2–Ne by DFT calculations using an ECP for Bi. Attractive potential minima surround the head-on position of the diatomic bismuth. The van der Waals radius is indicated by dashed lines for Bi and Ne.

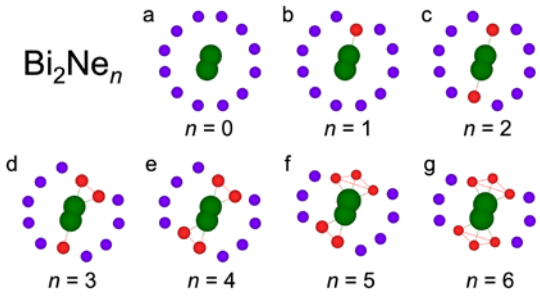

Fig. 7. Schematic views for possible arrangements of neighboring Ne atoms for Bi_2. Within a vacancy of the solid neon matrix, the dimer, Bi_2, is free-standing in (a), sticking head-on to one Ne atom in (b), and supported head-on by two Ne atoms in (c). The number of Ne atoms attached to Bi_2 is increasing one by one from three to six in (d), (e), (f), and (g).

ν_{00} = 17719 cm^{-1} of Bi_2, though the intensity is relatively weak. (2) Regularity for the increment of ~10 cm^{-1} is a key feature to be explained. Some relevant phenomena might be quantized vibration of weakly bound Bi_2–Ne, hindered rotation of Bi_2 in a vacancy of crystalline neon, and/or translational motion of Bi_2 in the trapping site of solid Ne. But, the next point to be explained brings a difficulty for these quantized nuclear motions. (3) The limited number of satellites, or the number of resonances, associated with a particular vibronic band restricts a model for the explanation.

Additional degrees of freedom are acquired by taking a bound state between diatomic bismuth and neon atoms into account. Usual site effects are associated with different trapping sites in which a different arrangement of surrounding neon atoms gives rise to different energy levels both in the upper and lower electronic states, thus showing a group of frequency-shifted transitions. For a possibility of stabilization of Bi_2 by the attachment of Ne atoms, Fig. 6 illustrates a calculated potential surface of Bi_2Ne. The attractive potential is located around the head-on position about the molecular axis of Bi_2. Stabilization energy is calculated to be 10–100 cm^{-1} along the line of the Bi–Bi bond depending on the theory and the basis set used, to get stabilized as a linear form of Bi–Bi–Ne. For the side-on position to have a triangular form, only a saddle point is found along the trench for a Ne atom and is not a local minimum. Dispersion corrections may improve the shape and depth of the potential surface.

5.3. *Clusters of* Bi_2Ne_n (n = 0–6)

Considerations on the above observations and calculations led us to propose a simple model of electronic energy shifts depending on the number of attached neon atoms to a diatomic molecule of bismuth. Figure 7 illustrates the idea of possible arrangements of Ne atoms around a Bi_2 molecule. Depending on the number of Ne atoms, n, which are intimately interacting with the Bi_2 molecule, weakly bound clusters are denoted as Bi_2Ne_n (n = 0–6). For n = 0, the Bi_2 molecule is free-standing in a vacancy of solid Ne with almost no gain for energy stabilization compared to the condition in the gas phase. Possible correction for the matrix condition relative to the vacuum will be the dielectric effect of solid Ne.

Table 2 compares the electronic term energy and harmonic frequencies reported so far. The observed frequency at 17738 cm^{-1} for the low-energy satellite, *a*, in solid Ne in Fig. 5 is close to the frequency for the origin band at ν_{00} = = 17719 cm^{-1} in the gas phase [1,4]. On the other hand, the strong peak, *b*, observed as the resonance excitation at 17790 cm^{-1} is closely located to the reported transition in solid Ne [9], within the error bar of the experiment. The term energy for the *A* state in solid Ne, T_e = 17806 cm^{-1} [9], is higher by ~67 cm^{-1} compared to that in the gas phase, T_e = 17739 cm^{-1} [1,4]. The difference seems to be large for a matrix shift of neon. There must be a mechanism of stabilization for the ground state, *X*, compared to that for the excited state, *A*, in solid Ne.

For a possible mechanism of stabilization for the ground-state Bi_2 in solid Ne, formation of the clusters, Bi_2Ne_n, is conceivable. Since the energy minimum for a Ne atom around the Bi_2 molecule is located on the molecular axis as depicted in Fig. 6, the cluster of Bi_2–Ne takes a linear form. For this configuration, the Bi_2 molecule is sticking head-on to a Ne atom in a vacancy of solid Ne as illustrated in Fig. 7(b). If the difference in stabilization between the ground *X* and excited *A* states is ~ 50 cm^{-1}, the model of Bi_2Ne fits well with the major peak, *b*, in Fig. 5. The strongest emission intensity of the peak, *b*, in Fig. 5 is rationalized by the idea of the largest population for this monoatomic coordination by a Ne atom, i.e., most Bi_2 molecules in solid Ne is suspended head-on by a nearest Ne atom.

Table 2. Molecular constants in cm^{-1} for the A–X transition of Bi_2

		T_e	$\omega'_e(A)$	$\omega''_e(X)$
Gerber*	gas	17739.3	132.49 ± 0.22	172.71 ± 0.27
Bondybey**	Ne	17806	134	173
This work	Ne	17811 ± 1.4	137 ± 1.2	174.2 ± 0.5

Notes: *Ref. 4: G. Gerber *et al.*, *J. Chem. Phys.* **64**, 3410 (1976); **Ref. 9: V. E. Bondybey *et al.*, *Chem. Phys. Lett.* **76**, 30 (1980).

Further stabilization is obtained by the attachment of the second Ne atom, again at the head-on position but the opposite side forming the linear cluster, Ne–Bi–Bi–Ne. This configuration is illustrated as Bi_2Ne_n of n = 2 in Fig. 7(c). Additional gain for stabilization is expected to be ~30 cm^{-1}, provided that the satellite, *c*, in Fig. 5 corresponds to the excitation followed by emission by Bi_2Ne_2. Fully occupied by two Ne atoms at the most stable positions along the molecular axis, the additional Ne atom should be accommodated in the same trench of the potential as the one already occupied by one Ne atom forming triply coordinated species, Bi_2Ne_3, as schematically illustrated in Fig. 7(d). The additional gain for stabilization must be small as ~10 cm^{-1}, when the satellite, *d*, in Fig. 5 is supposed to be corresponding. Similarly, the fourth and fifth Ne atoms are coordinating to Bi_2 as illustrated in Figs. 7(e) and 7(f), forming Bi_2Ne_4 and Bi_2Ne_5 for possible carriers of satellites, *e* and *f*, in Fig. 5, respectively. Additive gain for stabilization is again ~ 10 cm^{-1} for each, n = 4 and 5. The sixth Ne atom attaching to a Bi_2 molecule closes the first shell of the cluster of Bi_2Ne_n with the same energy gain of ~ 10 cm^{-1}. Further attachment of a Ne atom is impossible or results in no gain for the energy of stabilization. As Bi_2Ne_6, the diatomic bismuth is fully coordinated by six Ne atoms as illustrated in Fig. 7(g) for a candidate of the carrier of the satellite, *g*, in Fig. 5. A relatively strong emission of the signal, *g*, in Fig. 5 indicates the larger population of the carrier than those for the other satellites, *a* and *c*–*f*, in Fig. 5. This fully coordinated Bi_2Ne_6 is to be realized in a tightly packed trapping site in solid Ne. In contrast, the major progression of intense 0–v'' peaks, namely *b*, in Fig. 5 is noted again as due to the carrier of singly coordinated Bi_2Ne, which is bound head-on to a Ne atom exposed on the surface of a larger vacancy in solid Ne.

Finally, it is worth mentioning about previous observation of near infrared (NIR) emission spectra of triatomic bismuth, Bi_3, in solid Ne at 3 K [16]. The electronic transition with the origin band at 6600 cm^{-1} is accompanied by four satellites again with an increment of ~10 cm^{-1}. These satellites were thought of as discrete phonon levels of Bi_3 in a vacancy of solid Ne. But now, another idea emerges as the trapping sites having a different number of Ne atoms attaching to Bi_3, resulting in shifted energy levels in the upper and lower electronic states. The energy gain of ~10 cm^{-1} seems to be rather small but is apparently large for nonpolar homonuclear diatomic molecule. This may be possible for the largely polarizable heaviest stable element of bismuth. If we are allowed to mention the series of carriers, Bi_2Ne_n (n = 1–6), proposed in this work as novel species having bound electronic states, the idea will open a way to a new class of chemical compounds with the light noble gas atoms of neon, beyond xenon, krypton, and argon [33–45].

6. Conclusions

The A–X system of Bi_2 was revisited by laser induced fluorescence in solid Ne at 3 K. From the transition energies of 0–v'' bands (v'' = 5–12) in the emission spectra with the excitation of v'–0 bands (v' = 0–5), molecular constants are derived for the ground X state as well as for the excited A state to reproduce the reported ones in solid Ne. The 2D mapping of the emission spectra confirmed a series of satellites for each vibronic band in the A–X system. In considerations on stabilization by the interaction with Ne atoms, the satellite in the optical emission was proposed as a result of the excitation and emission by the cluster, Bi_2Ne_n (n = 0–6). The difference in the transition energy by ~50, ~30, and ~10 cm^{-1} observed for the series of satellites was attributed to the difference in the stabilization energy for the ground and excited electronic energy levels of X and A for Bi_2Ne_n. In conclusion, the diatomic bismuth, Bi_2, was revealed to present mostly as singly coordinated weakly bound cluster of Bi_2Ne in the cold rare gas matrix of solid neon.

Acknowlegments

This work was supported by the MEXT-Supported Program for the Strategic Research Foundation at Private Universities entitled Establishing a Best-Energy-Mix Research Center to Promote the Use of Solar Energy subsidized from the Ministry of Education, Culture, Sports, Science and Technology (MEXT) of Japan and Kindai University.

1. R.F. Barrow, F. Taher, J. d'Incan, C. Effantin, A.J. Ross, A. Topouzkhanian, G. Wannous, and J. Vergès, *Mol. Phys.* **87**, 725 (1996).
2. C. Effantin, A. Topouzkhanian, J. Figuet, J. d'Incan, R.F. Barrow, and J. Vergès, *J. Phys. B* **15**, 3829 (1982).
3. G.M. Almy and F.M. Sparks, *Phys. Rev.* **44**, 365 (1933).
4. G. Gerber, K. Sakurai, and H.P. Broida, *J. Chem. Phys.* **64**, 3410 (1976).
5. G. Gerber and H.P. Broida, *J. Chem. Phys.* **64**, 3423 (1976).
6. S. Drosch and G. Gerber, *J. Chem. Phys.* **77**, 123 (1982).

7. R.A. Teichman and E.R. Nixon, *J. Chem. Phys.* **67**, 2470 (1977).
8. V.E. Bondybey and J.H. English, *J. Chem. Phys.* **73**, 42 (1980).
9. V.E. Bondybey, G.P. Schwartz, J.E. Griffiths, and J.H. English, *Chem. Phys. Lett.* **76**, 30 (1980).
10. F. Ahmed and E.R. Nixon, *J. Chem. Phys.* **74**, 2156 (1981).
11. F. Ahmed and E.R. Nixon, *J. Chem. Phys.* **75**, 110 (1981).
12. K. Manzel, U. Engelhardt, H. Abe, W. Schulze, and F.W. Froben, *Chem. Phys. Lett.* **77**, 514 (1981).
13. B. Eberle, H. Sontag, and R. Weber, *Surf. Sci.* **156**, 751 (1985).
14. B. Eberle, H. Sontag, and R. Weber, *Chem. Phys.* **92**, 417 (1985).
15. T. Wakabayashi, M. Tomioka, Y. Wada, Y. Miyamoto, J. Tang, K. Kawaguchi, S. Kuma, N. Sasao, H. Nanjo, S. Uetake, M. Yoshimura, and I. Nakano, *Eur. Phys. J. D* **67**, 36 (2013).
16. T. Wakabayashi, Y. Wada, K. Nakajima, Y. Morisawa, S. Kuma, Y. Miyamoto, N. Sasao, M. Yoshimura, T. Sato, and K. Kawaguchi, *J. Phys. Chem. A* **119**, 2644 (2015).
17. M.L. Polak, J. Ho, G. Berber, and W.C. Lineberger, *J. Chem. Phys.* **95**, 3053 (1991).
18. C.A. Arrington and M.D. Morse, *J. Phys. Chem. B* **112**, 16182 (2008).
19. K. Balasubramanian and D.-W. Liao, *J. Chem. Phys.* **95**, 3064 (1991).
20. K. Balasubramanian, K. Sumathi, and D. Dai, *J. Chem. Phys.* **95**, 3494 (1991).
21. H. Zhang and K. Balasubramanian, *J. Chem. Phys.* **97**, 3437 (1992).
22. K.K. Das, H.-P. Liebermann, R.J. Buenker, and G. Hirsch, *J. Chem. Phys.* **102**, 4518 (1995).
23. H. Choi, C. Park, and K.K. Baeck, *J. Phys. Chem. A* **106**, 5177 (2002).
24. J.M. Jia, G.B. Chen, D.N. Shi, and B.L. Wang, *Eur. Phys. J. D* **47**, 359 (2008).
25. H.K. Yuan, H. Chen. A.L. Kuang, Y. Miao, and Z.H. Xiong, *J. Chem. Phys.* **128**, 094305 (2008).
26. L. Gao, P. Li, H. Lu, S.F. Li, and Z.X. Guo, *J. Chem. Phys.* **128**, 194304 (2008).
27. M. Gausa, R. Kaschner, G. Seifert, J.H. Faehrmann, H.O. Lutz, and K.-H. Meiwes-Broer, *J. Chem. Phys.* **104**, 9719 (1996).
28. R. Kelting, A. Baldes, U. Schwartz, T. Rapps, D. Schooss, P. Weis, C. Neiss, F. Weigend, and M.M. Kappes, *J. Chem. Phys.* **136**, 154309 (2012).
29. A. Fukumi, S. Kuma, Y. Miyamoto, K. Nakajima, I. Nakano, H. Nanjo, C. Ohae, N. Sasao, M. Tanaka, T. Taniguchi, S. Uetake, T. Wakabyashi, T. Yamaguchi, M. Yoshimi, and M. Yoshimura, *Prog. Theor. Exp. Phys.* 04D002 (2012).
30. T. Wakabayashi, A.-L. Ong, and W. Krätschmer, *J. Chem. Phys.* **116**, 5996 (2002).
31. P.M. Morse, *Phys. Rev.* **34**, 57 (1929).
32. Gaussian 16, Revision A.03, M.J. Frisch, G.W. Trucks, H.B. Schlegel, G.E. Scuseria, M.A. Robb, J.R. Cheeseman, G. Scalmani, V. Barone, G.A. Petersson, H. Nakatsuji, X. Li, M. Caricato, A.V. Marenich, J. Bloino, B.G. Janesko, R. Gomperts, B. Mennucci, H.P. Hratchian, J.V. Ortiz, A.F. Izmaylov, J.L. Sonnenberg, D. Williams-Young, F. Ding, F. Lipparini, F. Egidi, J. Goings, B. Peng, A. Petrone, T. Henderson, D. Ranasinghe, V.G. Zakrzewski, J. Gao, N. Rega, G. Zheng, W. Liang, M. Hada, M. Ehara, K. Toyota, R. Fukuda, J. Hasegawa, M. Ishida, T. Nakajima, Y. Honda, O. Kitao, H. Nakai, T. Vreven, K. Throssell, J.A. Montgomery, Jr., J.E. Peralta, F. Ogliaro, M.J. Bearpark, J.J. Heyd, E.N. Brothers, K.N. Kudin, V.N. Staroverov, T.A. Keith, R. Kobayashi, J. Normand, K. Raghavachari, A.P. Rendell, J.C. Burant, S.S. Iyengar, J. Tomasi, M. Cossi, J.M. Millam, M. Klene, C. Adamo, R. Cammi, J.W. Ochterski, R.L. Martin, K. Morokuma, O. Farkas, J.B. Foresman, and D.J. Fox, Gaussian, Inc., Wallingford CT, 2016.
33. M. Pettersson, J. Lundell, and M. Räsänen, *J. Chem. Phys.* **102**, 6423 (1995).
34. M. Pettersson, J. Lundell, and M. Räsänen, *J. Chem. Phys.* **103**, 205 (1995).
35. M. Pettersson, J. Nieminen, L. Khriachtchev, and M. Räsänen, *J. Chem. Phys.* **107**, 8423 (1997).
36. M. Pettersson, J. Lundell, L. Khriachtchev, and M. Räsänen, *J. Chem. Phys.* **109**, 618 (1998).
37. M. Pettersson, J. Lundell, L. Khriachtchev, E. Isoniemi, and M. Räsänen, *J. Am. Chem. Soc.* **120**, 7979 (1998).
38. M. Pettersson, J. Lundell, and M. Räsänen, *Eur. J. Inorg. Chem.* 729 (1999).
39. L. Khriachtchev, M. Pettersson, N. Runeberg, J. Lundell, and M. Räsänen, *Nature* **406**, 874 (2000).
40. J. Lundell, L. Khriachtchev, M. Pettersson, and M. Räsänen, *Fiz. Nizk. Temp.* **26**, (2000) [*Low. Temp. Phys.* **26**, 680 (2000)].
41. L. Khriachtchev, M. Pettersson, A. Lignell, and M. Räsänen, *J. Am. Chem. Soc.* **123**, 8610 (2001).
42. L. Khriachtchev, H. Tanskanen, J. Lundell, M. Pettersson, H. Kiljunen, and M. Räsänen, *J. Am. Chem. Soc.* **125**, 4696 (2003).
43. L. Khriachtchev, H. Tanskanen, A. Cohen, R.B. Gerber, J. Lundell, M. Pettersson, H. Kiljunen, and M. Räsänen, *J. Am. Chem. Soc.* **125**, 6876 (2003).
44. L. Khriachtchev, K. Isokoski, A. Cohen, M. Räsänen, and R.B. Gerber, *J. Am. Chem. Soc.* **130**, 6114 (2008).
45. L. Khriachtchev, M. Räsänen, and R.B. Gerber, *Acc. Chem. Res.* **42**, 183 (2009).

Bi_2Ne: слабкозв'язаний кластер двоатомного вісмуту з неоном

A. Endo, M. Hatanaka, N. Ueno, Y. Morisawa, and T. Wakabayashi

За допомогою лазерно-індукованої флуоресценції у твердому Ne при температурі 3 K вивчено перехід у двоатомному вісмуті Bi_2. Встановлено, що молекулярні константи, тобто коливальні частоти 137 $см^{-1}$ та 174 $см^{-1}$ для верхнього і нижнього електронних станів відповідають даним, які отримані Bondybey *et al*. [*Chem. Phys. Lett*. **76**, 30 (1980)]. Двовимірна картина спектру випромінювання підтвердила наявність смуг-сателітів, які відповідні за більш високу і більш низьку енергії збудження/випромінювання для кожної з основних смуг коливального ряду $v'–v''$ (v' = 0–5, v'' = 5–12). На підставі молекулярно-орбітальних розрахунків припускається, що спостережені сателіти обумовлені присутністю кластерів Bi_2Ne_n (n = 1–6). Відносно велике матричне зміщення ~ 67 $см^{-1}$ у твердому Ne для терма енергії в стані A може свідчити про існування двоатомного вісмуту у вигляді лінійно скоординованого кластера Bi_2Ne_n (n = 1–6) в матриці.

Ключові слова: зв'язаний кластер, флуоресценція, двоатомний вісмут.

Bi_2Ne: Слабосвязанный кластер двухатомного висмута с неоном

A. Endo, M. Hatanaka, N. Ueno, Y. Morisawa, and T. Wakabayashi

С помощью лазерно-индуцированной флуоресценции в твердом Ne при температуре 3 K изучен $A–X$ переход в двухатомном висмуте Bi_2. Установлено, что молекулярные константы, т.е. колебательные частоты 137 $см^{-1}$ и 174 $см^{-1}$ для верхнего и нижнего электронных состояний соответствуют данным, полученным Bondybey *et al*. [*Chem. Phys. Lett*. **76**, 30 (1980)]. Двумерная картина спектра излучения подтвердила наличие полос-сателлитов, соответствующих более высокой и более низкой энергиям возбуждения/излучения для каждой из основных полос колебательного ряда $v'–v''$ (v' = 0–5, v'' = = 5–12). На основании молекулярно-орбитальных расчетов предполагается, что наблюдаемые сателлиты обусловлены присутствием кластеров Bi_2Ne_n (n = 1–6). Относительно большое матричное смещение ~67 $см^{-1}$ в твердом Ne для терма энергии в состоянии A может свидетельствовать о существовании двухатомного висмута в виде линейно скоординированного кластера Bi_2Ne_n (n = 1–6) в матрице.

Ключевые слова: связанный кластер, флуоресценция, двухатомный висмут.